LETTERS

A modular switch for spatial Ca^{2+} selectivity in the calmodulin regulation of Ca_V channels

Ivy E. Dick[1]*, Michael R. Tadross[1]*, Haoya Liang[1], Lai Hock Tay[1], Wanjun Yang[1] & David T. Yue[1]

Ca^{2+}/calmodulin-dependent regulation of voltage-gated Ca_V1–2 Ca^{2+} channels shows extraordinary modes of spatial Ca^{2+} decoding and channel modulation[1–6], vital for many biological functions[6–9]. A single calmodulin (CaM) molecule associates constitutively with the channel's carboxy-terminal tail[3,10–13], and Ca^{2+} binding to the C-terminal and N-terminal lobes of CaM can each induce distinct channel regulations[2,14]. As expected from close channel proximity, the C-lobe responds to the roughly 100-μM Ca^{2+} pulses driven by the associated channel[15,16], a behaviour defined as 'local Ca^{2+} selectivity'. Conversely, all previous observations have indicated that the N-lobe somehow senses the far weaker signals from distant Ca^{2+} sources[2,3,17,18]. This 'global Ca^{2+} selectivity' satisfies a general signalling requirement, enabling a resident molecule to remotely sense cellular Ca^{2+} activity, which would otherwise be overshadowed by Ca^{2+} entry through the host channel[5,6]. Here we show that the spatial Ca^{2+} selectivity of N-lobe CaM regulation is not invariably global but can be switched by a novel Ca^{2+}/CaM-binding site within the amino terminus of channels (NSCaTE, for N-terminal spatial Ca^{2+} transforming element). Native $Ca_V2.2$ channels lack this element and show N-lobe regulation with a global selectivity. On the introduction of NSCaTE into these channels, spatial Ca^{2+} selectivity transforms from a global to local profile. Given this effect, we examined $Ca_V1.2$/$Ca_V1.3$ channels, which naturally contain NSCaTE, and found that their N-lobe selectivity is indeed local. Disruption of this element produces a global selectivity, confirming the native function of NSCaTE. Thus, differences in spatial selectivity between advanced Ca_V1 and Ca_V2 channel isoforms are explained by the presence or absence of NSCaTE. Beyond functional effects, the position of NSCaTE on the channel's amino terminus indicates that CaM can bridge the amino terminus and carboxy terminus of channels. Finally, the modularity of NSCaTE offers practical means for understanding the basis of global Ca^{2+} selectivity[19].

Figure 1a, b shows a prototypic example of global Ca^{2+} regulation induced by Ca^{2+} binding to the N-lobe of CaM, here driving Ca^{2+}-dependent inactivation (CDI) of $Ca_V2.2$ channels[3]. On channel activation by a depolarizing voltage step (Fig. 1a), this CDI manifests itself as an accelerated decay of Ca^{2+} (middle, red trace) against Ba^{2+} current (black trace). The baseline decay in Ba^{2+}, which binds poorly to CaM[2], reflects a separate voltage-dependent inactivation process[7]. In population data (Fig. 1a, right), the fraction of peak Ca^{2+} current remaining after a 300-ms depolarization, r_{300}, is a U-shaped function of voltage (red circles), providing a hallmark of CDI[20]. The corresponding Ba^{2+} relation (Fig. 1a, black circles) shows a weak monotonic decline, and the difference between Ca^{2+} and Ba^{2+} relations (f_{300}) quantifies pure CDI[20]. In accord with a so-far invariant rule[3,6], N-lobe regulation of Ca^{2+} channels is selective for a global Ca^{2+} increase arising from spatially distant sources. Such global crosstalk is permitted under modest intracellular Ca^{2+} buffering[18] that approximates physiological conditions (Fig. 1a, left, shading with 0.5 mM EGTA). Thus, strong buffering that localizes Ca^{2+} to channel nanodomains[15,16] (Fig. 1b, left, small hemisphere in 10 mM BAPTA) almost eliminates CDI (Fig. 1b, middle and right).

Previous splice variations, mutations and chimaeras have at best altered the strength of such CDI[2,3,21], making global Ca^{2+} preference seem immutable. Here, however, when the N terminus of $Ca_V1.2$ channels (NT_C) was substituted into $Ca_V2.2$, the resulting 'cBBBBb' chimaera showed strong N-lobe CDI in high buffering (Fig. 1c and Supplementary Information). Introducing NT_C into $Ca_V2.1$ produced an analogous result (data not shown), thus generalizing the effect across the Ca_V2 family. This conversion to local Ca^{2+} selectivity is unprecedented, especially given the preponderance of known structural determinants for CDI on the carboxy termini of channels[22].

To explore the basis of this effect, we undertook progressive amino-terminal deletions from the NT_C segment within the cBBBBb chimaera. Deletion of the first 81 residues (Δ82cBBBBb) completely spared CDI in high buffering (Fig. 1d, top left, where the grey trace shows the full-length NT_C profile). By contrast, removing just one more residue (82W) significantly decreased CDI (Fig. 1d, top middle), and additional deletion further suppressed CDI (Fig. 1d, top right). Explicit correlation of CDI strength with NT_C deletion corroborated these trends (Fig. 1d, bottom, left axis, circles), localizing the impact to a short contiguous region (yellow highlight).

What could the essential mechanistic ingredient of this locus be? We reasoned that this segment might orchestrate special molecular interactions with cytoplasmic channel loops or modulatory ligands, and thus probed for such associations with the use of a live-cell fluorescence resonance energy transfer (FRET) two-hybrid assay[13]. Using this approach, with enhanced yellow fluorescent protein fused to CaM (EYFP–CaM), and enhanced cyan fluorescent protein (ECFP) to various portions of NT_C or the $Ca_V2.2$ amino terminus (NT_B), we found a unique ability of NT_C to bind Ca^{2+}/CaM within the intracellular milieu of HEK-293 cells (Fig. 1e). To start with, NT_B failed to display FRET interaction with CaM, either in the Ca^{2+}-free or the Ca^{2+}-bound state (Fig. 1e, middle column, topmost bars). Specifically, the optical parameter FRET ratio (FR) was about 1, signifying the absence of FRET[13]. By contrast, NT_C clearly interacted with Ca^{2+}/CaM ($FR \approx 2$), but not apoCaM (Ca^{2+}-free CaM). Trisection of NT_C localized Ca^{2+}/CaM binding to the middle third (Fig. 1e, middle column, residues 67–131), and further deletions identified a sharp decrease in FRET on removal of W82 (Supplementary Information). Because FR depends on the fractional binding between interacting partners, cell-to-cell variation in expression permitted the resolution of binding curves, each specifying a relative

[1]Calcium Signals Laboratory, Departments of Biomedical Engineering and Neuroscience, The Johns Hopkins University School of Medicine, Ross Building, Room 713, 720 Rutland Avenue, Baltimore, Maryland 21205, USA.
*These authors contributed equally to this work.

dissociation constant $K_{d,EFF}$ (ref. 13) (Fig. 1e, right column, arrow). Alignments of these NT_C fragments and their $K_{d,EFF}$ values (Fig. 1d, squares, and Supplementary Information) localized a CaM-binding segment that coincided well with the critical CDI segment (Fig. 1d, yellow highlight). In particular, a W82A point mutation suppressed the interaction of Ca^{2+}/CaM with NT_C (Fig. 1f), fitting with the decrease in CDI of the corresponding channel truncation (Fig. 1d, top row, middle). Thus, the transformation of spatial Ca^{2+} selectivity is correlated with a previously unrecognized Ca^{2+}/CaM interaction site within NT_C.

This connection was deepened in two ways (Fig. 2). First, the *in situ* FRET approach was confirmed by *in vitro* assays, pairing purified Ca^{2+}/CaM with a synthetic peptide (SWQAAIDAARQAKLMGSA) spanning the key NT_C binding region. Without peptides, CaM migrated rapidly under non-denaturing PAGE[2] (Fig. 2a, left, lane 1, open arrowhead). When fully complexed with the IQ domain peptide of $Ca_V2.1$ (IQ_A), CaM showed a known slowing of mobility[2] (Fig. 2a, left, lane 2, filled arrowhead). Increasing $NT_{C\text{-peptide}}$ produced progressive conversion to the faster mobility species (Fig. 2a, left, lanes 3–8), indicating competitive binding to CaM. By contrast, a mutant W82A peptide ($NT_{C\text{-peptide-(W82A)}}$; Fig. 2a, right) was unable to bind CaM. More quantitatively, $NT_{C\text{-peptide}}$ depressed the emission spectrum of dansylated CaM (Fig. 2b, inset), allowing the resolution of a 1:1 binding curve with a K_d of 1.2 μM (Fig. 2b, filled symbols). $NT_{C\text{-peptide-(W82A)}}$ showed no such interaction (Fig. 2b, open symbols). These *in vitro* assays established direct Ca^{2+}/CaM binding to the NT_C core region.

Second, further in-depth mapping refined the correlation between spatial Ca^{2+} selectivity and CaM binding to NT_C. Alanine point mutations were introduced into the NT_C domain of cBBBBb channels, targeting key sites inferred from a preliminary report[19]. These manipulations decreased CDI (in high buffering) with the rank order W82A > I86A > R90A (Fig. 2c). Reassuringly, these changes in CDI (f_{300}) correlated closely with the relative dissociation constant ($K_{d,EFF}$) for CaM interaction with corresponding mutant NT_C peptides, as determined by FRET (Fig. 2d and Supplementary Information). Given the strong function and affiliation with CaM binding to the core NT_C locus, we named this element NSCaTE (Fig. 2c, top).

Although this module impacts chimaeric channels, does NSCaTE function within naturally occurring channels? Alignments of various Ca_V1–2 Ca^{2+} channels (Fig. 3a) revealed that NSCaTE is present not only in $Ca_V1.2$ (α_{1C}), but also $Ca_V1.3$ (α_{1D}). Our attention was initially drawn to NSCaTE in $Ca_V1.3$ because these channels show two distinct and robust forms of CDI, each selectively triggered by Ca^{2+} binding to a different lobe of CaM[14]. As a preliminary test for the functionality of the $Ca_V1.3$ NSCaTE, we checked for Ca^{2+}/CaM interaction (Fig. 3b). FRET assays showed selective interaction of Ca^{2+}/CaM with the midsection of the $Ca_V1.3$ amino terminus (Fig. 3b; NT_D-(35–94)), yielding a $K_{d,EFF}$ on a par with those of NT_C analogues (Fig. 1e). Consistent with W82A effects in NT_C (Fig. 1f), mutation of the analogous tryptophan in NT_D (NT_D-W44A-(35–94)) eliminated Ca^{2+}/CaM interaction (Fig. 3b and Supplementary Information). Substituting NT_D into $Ca_V2.2$ (yielding the dBBBBb chimaera) also produced strong CDI in high buffering (Fig. 3c and Supplementary Information), confirming the transforming capacity of the $Ca_V1.3$ NSCaTE.

We next examined whether the intrinsic NSCaTE imparts local selectivity to the native $Ca_V1.3$, contrary to the current dogma that the N-lobe invariably senses global Ca^{2+}. In $Ca_V1.3$, the N-lobe form of CDI can be isolated by simultaneously expressing a mutant CaM

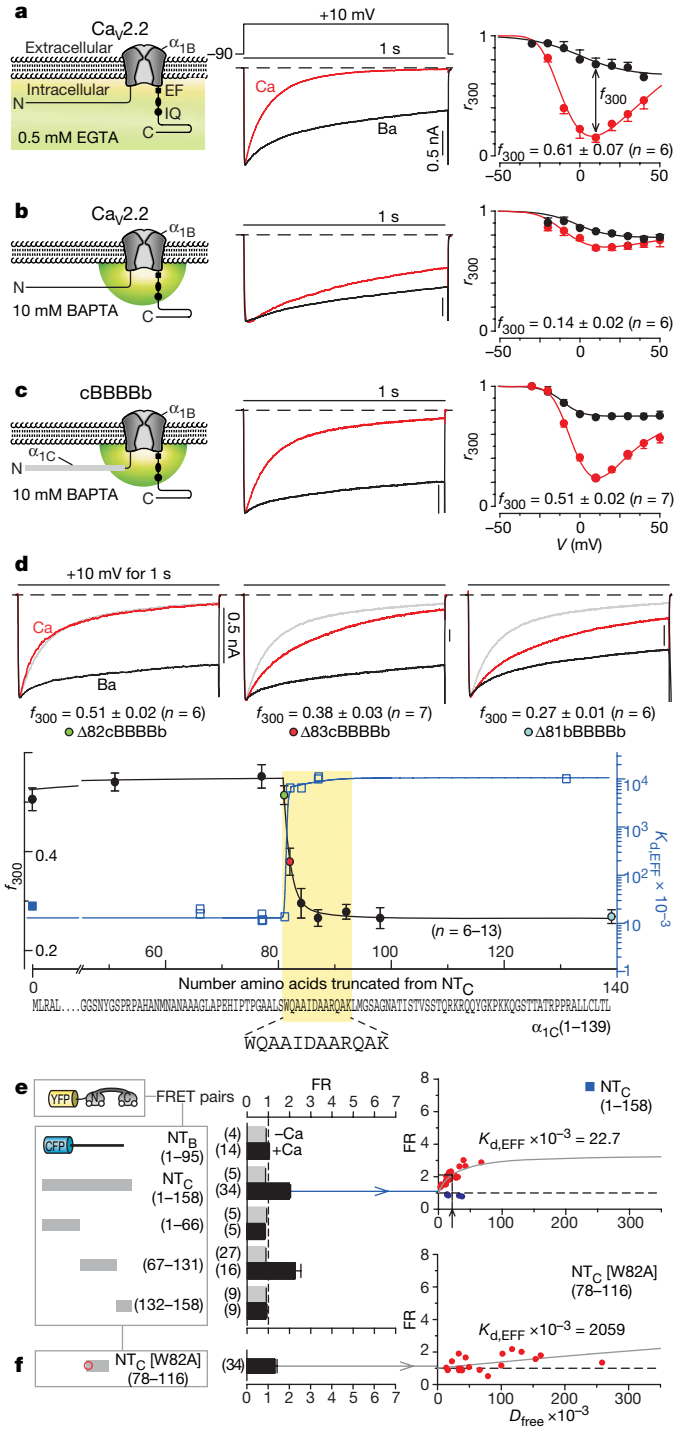

Figure 1 | Transformation of spatial Ca^{2+} selectivity in $Ca_V2.2$ channels. **a**, $Ca_V2.2$ CDI, low buffering. Left: diagram of global Ca^{2+} elevation. Middle: example traces in Ca^{2+} (red) and Ba^{2+} (black). Throughout, the current bar refers to the Ca^{2+} trace, and the Ba^{2+} trace is normalized to the Ca^{2+} peak. Right: average CDI; f_{300} at 10 mV; results are means ± s.e.m. throughout; cell numbers are shown in parentheses. **b**, $Ca_V2.2$ CDI, high buffering. Left: diagram of local Ca^{2+} signalling. **c**, CDI of cBBBBb. **d**, Localizing spatial Ca^{2+} transforming element (yellow highlight) within NT_C. Top: example currents for cBBBBb with N-terminal deletions, (Δ82cBBBBb, removal of first 81 residues of cBBBBb; Δ81bBBBBb, removal of entire amino terminus of $Ca_V2.2$). Middle: f_{300} (high buffering) versus residues deleted from cBBBBb; left axis and circles with colours correspond to examples above. $K_{d,EFF}$ is also plotted on same abscissa; blue right axis and blue squares, with filled symbol corresponding to **e**. Bottom: localized sequence for both CDI transformation and Ca^{2+}/CaM binding within NT_C (yellow highlight). **e**, **f**, FRET for YFP–CaM versus channel amino-terminal segments tagged with CFP. Left: construct schematics. Middle: FRET ratios (FR). Right: example binding curves, with red symbols for Ca^{2+}/CaM, and blue symbols for apoCaM (arrow in **e** shows $K_{d,EFF}$). D_{free}, relative concentration of CFP-tagged molecules[13]. **f**, Abolition of FRET between YFP–CaM and a CFP-tagged channel amino-terminal segment with a W82A mutation.

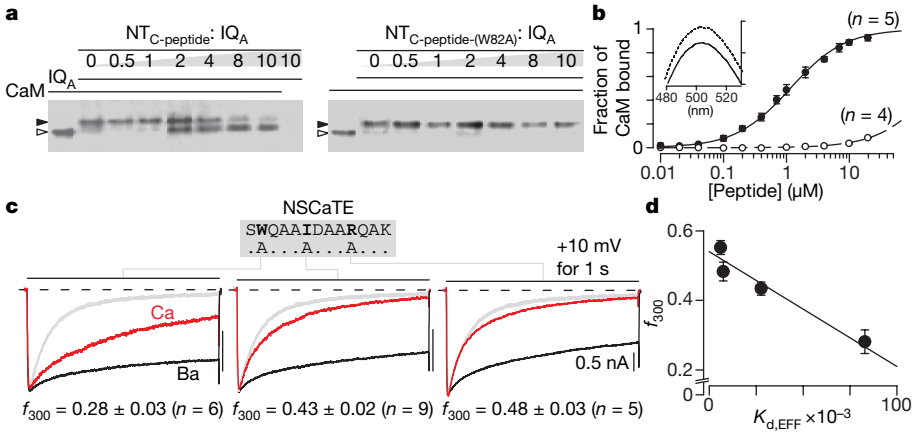

Figure 2 | Direct CaM binding and mapping of key NSCaTE residues. **a**, Competitive gel-mobility shift assay, confirming Ca^{2+}/CaM interaction with $NT_{C\text{-}peptide}$ (left), not mutant $NT_{C\text{-}peptide\text{-}(W82A)}$ (right). **b**, Dansylated Ca^{2+}/CaM spectrofluorimetry. Binding with $NT_{C\text{-}peptide}$ (filled circles), not with mutant $NT_{C\text{-}peptide\text{-}(W82A)}$ (open circles), both plotted as means ± s.e.m. Inset: $NT_{C\text{-}peptide}$ decreases the emission spectrum. **c**, CDI in high buffering, for Δ78cBBBBb channels with point mutations as labelled. Format as in Fig. 1a; the grey trace shows the baseline Δ78cBBBBb profile. **d**, Close correlation of CDI in high buffering with NT_C module affinity for Ca^{2+}/CaM_{34} (Supplementary Information).

(CaM_{34}) in which Ca^{2+} binding is restricted to the N-lobe[2,20]. So far, such CDI has been studied only under modest Ca^{2+} buffering[14]. Here, even under high buffering, N-lobe CDI was pronounced (Fig. 3d, top row). More tellingly, a W44A mutation within $Ca_V1.3$ almost eliminated this CDI (Fig. 3d, middle row), as did deletion of this region (Supplementary Information). To exclude indiscriminate disruption of CDI, we confirmed that CDI resurfaced under modest buffering permissive of global signalling (Fig. 3d, bottom row, and Supplementary Information). CDI was entirely CaM-mediated under decreased buffering[14] (Supplementary Information), and C-lobe CDI was unaffected by similar mutations[19]. Hence, the native $Ca_V1.3$ NSCaTE endows N-lobe CDI with a local selectivity, and decreasing Ca^{2+}/CaM binding to NSCaTE switches this selectivity towards a global profile.

Returning to native $Ca_V1.2$, coarse identification of Ca^{2+}/CaM binding to the N terminus of these channels has been reported, but the functional consequences have been unclear[23]. In particular, the CaM-mediated CDI of these channels has been attributed only to the C-lobe of CaM[7,20]; apparently absent has been an N-lobe form of CDI, the target of NSCaTE effects. Here, however, on simultaneous transfection of $Ca_V1.2$ with CaM_{34}, to isolate a potential N-lobe component, small but unmistakable CDI was seen during prolonged 1-s depolarization, even in high buffering (Fig. 3e, top row). In addition, a W82A mutation abolished this CDI (Fig. 3e, middle row), but

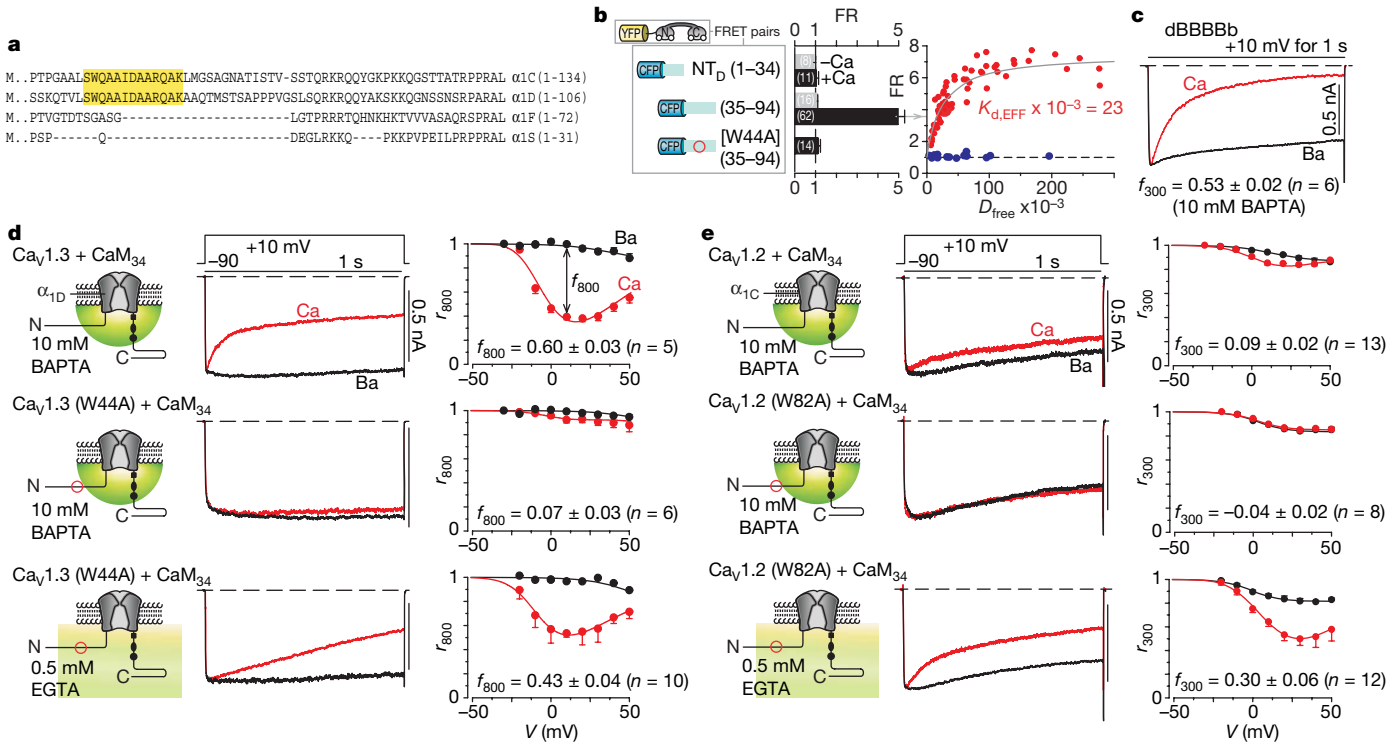

Figure 3 | NSCaTE transforms spatial Ca^{2+} selectivity in native Ca_V1 channels. **a**, α_1 alignment, Ca_V1 channels. **b**, FRET assays. Format as in Fig. 1e. **c**, CDI of dBBBBb in high buffering. **d**, Effect of native NSCaTE on N-lobe CDI of $Ca_V1.3$. Top: CDI persists in high buffering. Middle: CDI is eliminated by W44A mutation. Bottom: CDI reappears in W44A mutant under low buffering. Format as in Fig. 1a, except for 800-ms metrics. **e**, Native NSCaTE effects in $Ca_V1.2$. Format as in **d**, with 300-ms metrics.

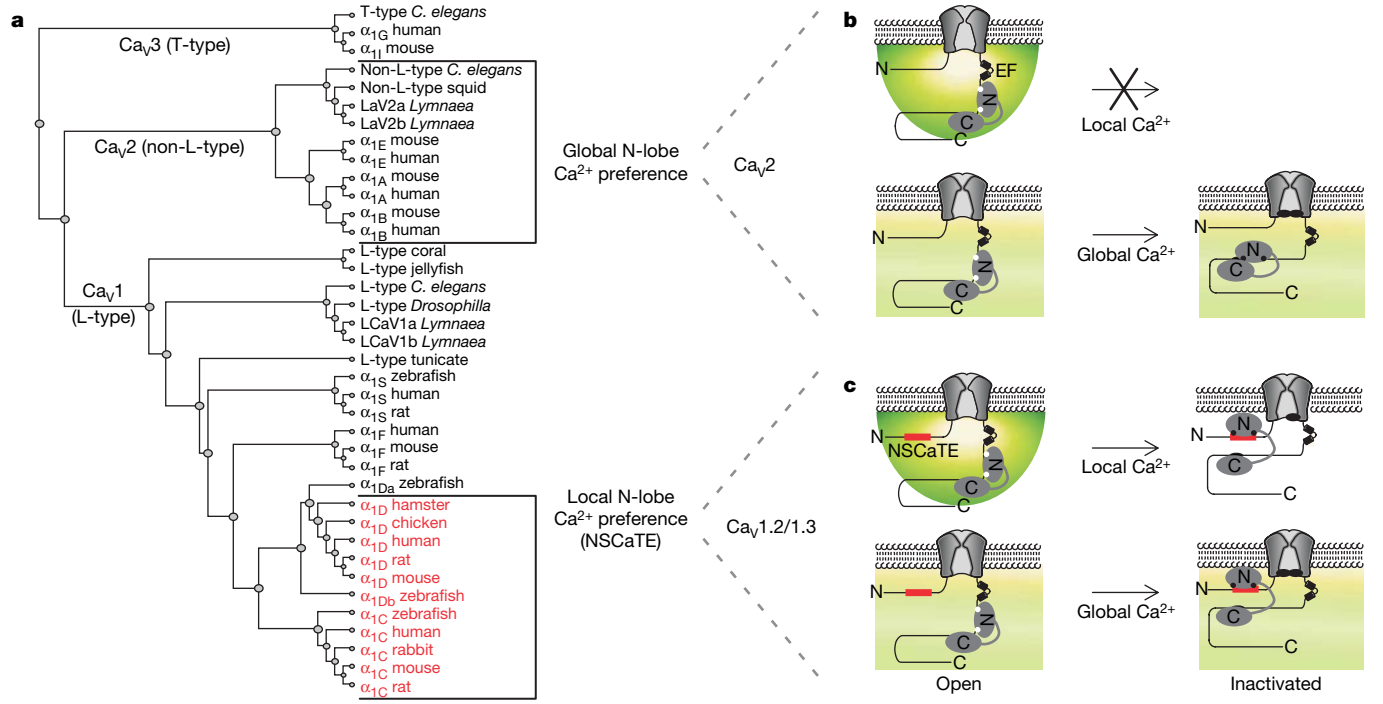

Figure 4 | Functional and structural properties for NSCaTE switching of spatial Ca^{2+} selectivity. **a**, Ca_V1–2 dendrogram, based on α_1 subunits (Supplementary Information). Red, NSCaTE-containing channels. **b**, Diagram of N-lobe CDI in Ca_V2 channels. Absence of NSCaTE yields global Ca^{2+} selectivity. Black circles on CaM, Ca^{2+} ions. **c**, N-lobe CDI in Ca_V1 channels that contain NSCaTE (red) show local Ca^{2+} selectivity. CaM bridges the amino and carboxy termini of inactivated channels (right).

spared it under global Ca^{2+} signalling (bottom row). A more drastic deletion of the native NSCaTE produced an identical effect (Supplementary Information). Again, the globally signalled CDI remained entirely CaM dependent (Supplementary Information). Hence, NSCaTE functions similarly in native $Ca_V1.2$ and $Ca_V1.3$; the weaker N-lobe CDI of $Ca_V1.2$ is expected from its lower open probability[19,24]. These results generalize the lessons of chimaeric channels to the operation of native channels and constitute the first examples in which the N-lobe of CaM shows local Ca^{2+} selectivity.

In all, the traditionally global spatial Ca^{2+} selectivity of channel regulation by the N-lobe[3,6] is not invariant but can be transformed towards a local selectivity by NSCaTE, a Ca^{2+}/CaM-binding site unrecognized by current motif-detection algorithms[25]. Four perspectives emerge. First, the presence of NSCaTE in $Ca_V1.2$ and $Ca_V1.3$—along with its absence from Ca_V2 channels—underlies the contrasting spatial Ca^{2+} preferences of N-lobe CDI between these two channel clades (Fig. 4a). Previously, N-lobe regulation had been viewed as always having a global Ca^{2+} selectivity[3,6], which is true for Ca_V2 channels (Fig. 4b). We now recognize that the analogous N-lobe CDI of $Ca_V1.2$/$Ca_V1.3$ channels[14] exhibits local selectivity, owing to an intrinsic NSCaTE (Fig. 4c). Second, NSCaTE promises vital adjustments of spatial selectivity in various biological contexts. NSCaTE would customize $Ca_V1.2$/1.3 regulation for local Ca^{2+} signalling in cardiac dyads[4,7], and for neuronal Ca^{2+} entry whose precise regulation is essential for long-term synaptic plasticity[26,27]. A naturally occurring $Ca_V1.2$ splice variant features a premature stop codon just after the channel's amino terminus[21]. The predicted protein product contains NSCaTE and may exert a dominant-negative effect. Although expressing NT_C and $Ca_V1.3$ together left CDI unchanged in HEK-293 cells (data not shown), additional mechanisms may exist in native tissues to render this splice product active. Third, unlike most functional motifs, which are pervasive from bacteria to advanced mammals[25], NSCaTE is found only in a subset of Ca_V1 channels from advanced species (Fig. 4a, red) and in multiple bacterial proteins (Supplementary Information). A prokaryotic NSCaTE from *Xanthomonas* may in fact bind endogenous CaM-like molecules (Supplementary Information), hinting that channel and bacterial motifs share a common heritage. Last, NSCaTE furnishes valuable structural and mechanistic insights. For structure, we deduce that CaM can bridge the carboxy and amino termini of $Ca_V1.2$/$Ca_V1.3$ channels (Fig. 4c, right), as follows. This study establishes Ca^{2+}-bound N-lobe interaction with NSCaTE on the channel's amino terminus. By contrast, previous reports emphasized that regulation by the C-lobe involves its Ca^{2+}-bound and Ca^{2+}-free interactions with the channel's carboxy terminus[12,20,28]. Moreover, a single resident CaM orchestrates both C-lobe and N-lobe regulation[10,11], where both coexist in $Ca_V1.2$/$Ca_V1.3$ channels[14,20]. Finally, the channel's amino and carboxy termini are in close proximity, and move with channel gating[29]. This bridging therefore seems probable, expanding a theme where the lobes of CaM crosslink separate parts of a molecule[30]. As for mechanism, the modularity of NSCaTE indicates that spatial Ca^{2+} preference is not hopelessly intertwined within holochannel structure. Manipulating this compact element promises to provide insights into the elusive mechanism underlying spatial Ca^{2+} selectivity[6,19].

METHODS SUMMARY

Molecular biology. Channel chimaeras, mutations and CFP/YFP-FRET constructs were prepared with standard molecular biology techniques.

Electrophysiology. Transient transfection of HEK-293 cells with recombinant channels, and whole-cell current recordings, were performed mostly as described previously[2].

CaM binding assays. FRET two-hybrid experiments were performed in HEK-293 cells as described[13]. Gel mobility-shift assays were conducted in accordance with protocols similar to those in our previous work[2,20]. Spectrofluorimetric determinations of dansyl-CaM interaction were conducted as outlined previously[2,3,20].

Full Methods and any associated references are available in the online version of the paper at www.nature.com/nature.

Received 30 July; accepted 6 December 2007.
Published online 30 January; corrected 14 February 2008 (details online).

1. Lee, A., Scheuer, T. & Catterall, W. A. Ca^{2+}/calmodulin-dependent facilitation and inactivation of P/Q-type Ca^{2+} channels. *J. Neurosci.* **20**, 6830–6838 (2000).

2. DeMaria, C. D., Soong, T. W., Alseikhan, B. A., Alvania, R. S. & Yue, D. T. Calmodulin bifurcates the local Ca^{2+} signal that modulates P/Q-type Ca^{2+} channels. *Nature* **411,** 484–489 (2001).
3. Liang, H. *et al.* Unified mechanisms of Ca^{2+} regulation across the Ca^{2+} channel family. *Neuron* **39,** 951–960 (2003).
4. Bootman, M. D., Lipp, P. & Berridge, M. J. The organisation and functions of local Ca^{2+} signals. *J. Cell Sci.* **114,** 2213–2222 (2001).
5. Evans, R. M. & Zamponi, G. W. Presynaptic Ca^{2+} channels—integration centers for neuronal signaling pathways. *Trends Neurosci.* **29,** 617–624 (2006).
6. Dunlap, K. Calcium channels are models of self-control. *J. Gen. Physiol.* **129,** 379–383 (2007).
7. Alseikhan, B. A., DeMaria, C. D., Colecraft, H. M. & Yue, D. T. Engineered calmodulins reveal the unexpected eminence of Ca^{2+} channel inactivation in controlling heart excitation. *Proc. Natl Acad. Sci. USA* **99,** 17185–17190 (2002).
8. Xu, J. & Wu, L. G. The decrease in the presynaptic calcium current is a major cause of short-term depression at a calyx-type synapse. *Neuron* **46,** 633–645 (2005).
9. Dolmetsch, R. E., Pajvani, U., Fife, K., Spotts, J. M. & Greenberg, M. E. Signaling to the nucleus by an L-type calcium channel–calmodulin complex through the MAP kinase pathway. *Science* **294,** 333–339 (2001).
10. Mori, M. X., Erickson, M. G. & Yue, D. T. Functional stoichiometry and local enrichment of calmodulin interacting with Ca^{2+} channels. *Science* **304,** 432–435 (2004).
11. Yang, P. S., Mori, M. X., Antony, E. A., Tadross, M. R. & Yue, D. T. A single calmodulin imparts distinct N- and C-lobe regulatory processes to individual $Ca_V1.3$ channels. *Biophys. J.*, Suppl. 354a, 1669-Plat (2007).
12. Pitt, G. S. *et al.* Molecular basis of calmodulin tethering and Ca^{2+}-dependent inactivation of L-type Ca^{2+} channels. *J. Biol. Chem.* **276,** 30794–30802 (2001).
13. Erickson, M. G., Liang, H., Mori, M. X. & Yue, D. T. FRET two-hybrid mapping reveals function and location of L-type Ca^{2+} channel CaM preassociation. *Neuron* **39,** 97–107 (2003).
14. Yang, P. S. *et al.* Switching of Ca^{2+}-dependent inactivation of $Ca_v1.3$ channels by calcium binding proteins of auditory hair cells. *J. Neurosci.* **26,** 10677–10689 (2006).
15. Augustine, G. J., Santamaria, F. & Tanaka, K. Local calcium signaling in neurons. *Neuron* **40,** 331–346 (2003).
16. Neher, E. Vesicle pools and Ca^{2+} microdomains: new tools for understanding their roles in neurotransmitter release. *Neuron* **20,** 389–399 (1998).
17. Chaudhuri, D., Issa, J. B. & Yue, D. T. Elementary mechanisms producing facilitation of $Ca_v2.1$ (P/Q-type) channels. *J. Gen. Physiol.* **129,** 385–401 (2007).
18. Song, L. S., Sham, J. S., Stern, M. D., Lakatta, E. G. & Cheng, H. Direct measurement of SR release flux by tracking 'Ca^{2+} spikes' in rat cardiac myocytes. *J. Physiol. (Lond.)* **512,** 677–691 (1998).
19. Tadross, M. R., Dick, I. E. & Yue, D. T. Mechanism of Ca^{2+} decoding by the CaM/Ca_V channel complex. *Biophys. J.*, Suppl. 354a, 1670-Plat (2007).
20. Peterson, B. Z., DeMaria, C. D., Adelman, J. P. & Yue, D. T. Calmodulin is the Ca^{2+} sensor for Ca^{2+}-dependent inactivation of L-type calcium channels. *Neuron* **22,** 549–558 (1999).
21. Tang, Z. Z. *et al.* Transcript scanning reveals novel and extensive splice variations in human l-type voltage-gated calcium channel, $Ca_v1.2\alpha_1$ subunit. *J. Biol. Chem.* **279,** 44335–44343 (2004).
22. Van Petegem, F., Chatelain, F. C. & Minor, D. L. Jr. Insights into voltage-gated calcium channel regulation from the structure of the $Ca_V1.2$ IQ domain-Ca^{2+}/calmodulin complex. *Nature Struct. Mol. Biol.* **12,** 1108–1115 (2005).
23. Ivanina, T., Blumenstein, Y., Shistik, E., Barzilai, R. & Dascal, N. Modulation of L-type Ca^{2+} channels by $G_{\beta\gamma}$ and calmodulin via interactions with N and C termini of α_{1C}. *J. Biol. Chem.* **275,** 39846–39854 (2000).
24. de Leon, M. *et al.* Essential Ca^{2+}-binding motif for Ca^{2+}-sensitive inactivation of L-type Ca^{2+} channels. *Science* **270,** 1502–1506 (1995).
25. Rhoads, A. R. & Friedberg, F. Sequence motifs for calmodulin recognition. *FASEB J.* **11,** 331–340 (1997).
26. Toescu, E. C. & Verkhratsky, A. The importance of being subtle: small changes in calcium homeostasis control cognitive decline in normal aging. *Aging Cell* **6,** 267–273 (2007).
27. Moosmang, S. *et al.* Role of hippocampal $Ca_v1.2$ Ca^{2+} channels in NMDA receptor-independent synaptic plasticity and spatial memory. *J. Neurosci.* **25,** 9883–9892 (2005).
28. Evans, J., Erickson, M. G., Anderson, M. J. & Yue, D. T. FRET-based mapping of calmodulin preassociation with P/Q-type Ca channels. *Biophys. J.*, Suppl. 84a, 2615-Pos (2003).
29. Kobrinsky, E., Schwartz, E., Abernethy, D. R. & Soldatov, N. M. Voltage-gated mobility of the Ca^{2+} channel cytoplasmic tails and its regulatory role. *J. Biol. Chem.* **278,** 5021–5028 (2003).
30. Drum, C. L. *et al.* Structural basis for the activation of anthrax adenylyl cyclase exotoxin by calmodulin. *Nature* **415,** 396–402 (2002).

Supplementary Information is linked to the online version of the paper at www.nature.com/nature.

Acknowledgements We thank H. Agler and M. Mori for early characterization of the cBBBBb chimaeric channel; C. Iwema and J. Pevsner for bioinformatics advice; K.-W. Yau, E. Young and members of the Calcium Signals Laboratory for comments. Supported by grants from the NINDS (to I.E.D.), the NIGMS (to M.R.T.), and the NIMH and NHLBI (to D.T.Y.).

Author Information Reprints and permissions information is available at www.nature.com/reprints. Correspondence and requests for materials should be addressed to D.T.Y. (dyue@bme.jhu.edu).

METHODS

Molecular biology. The $\alpha_{1cBBBBb}$ subunit was the published $\alpha_{1cBBBBb}$/pcDNA3 construct[31]. PCR was used to truncate the amino terminus of this construct: the forward primer, containing a unique *Eco*RI site and Kozak start, determined the extent of truncation; the reverse primer annealed downstream of a unique *Age*I site. PCR fragments were ligated into $\alpha_{1cBBBBb}$/pcDNA3 with *Eco*RI/*Age*I. Mutations to NSCaTE were introduced into the $\alpha_{1\Delta78cBBBBb}$ truncation construct (starts with the 78th residue of α_{1C}), using forward primers as above but containing desired mutations. For chimaeric $\alpha_{1dBBBBb}$, PCR introduced a silent and unique *Bsi*WI site at residue 83 of α_{1B}/pcDNA3, yielding α_{1B}_BsiWI$^+$. The amino terminus of α_{1D}[32] was amplified by PCR, then ligated into unique *Eco*RI and *Bsi*WI sites of α_{1B}_BsiWI$^+$, yielding $\alpha_{1dBBBBb}$. The α_{1B} ($Ca_V2.2$) used here is a variant of the human α_{1B} reported previously[33]; it is identical except for V354M and R369S variations. This variant backbone was used for all constructs, including $\alpha_{1dBBBBb}$ and the previously published $\alpha_{1cBBBBb}$/pcDNA3 (ref. 31). For completeness we confirmed that transforming NSCaTE effects were also present by using the more common α_{1B} backbone for $\alpha_{1cBBBBb}$ and $\alpha_{1dBBBBb}$. A 141-residue amino-terminal truncation of the $Ca_V1.2$ α_{1C} subunit ($\alpha_{1C[NT\Delta]}$) was generated by PCR, amplifying residues 142–611 from α_{1C} (ref. 34), followed by ligation into the parental α_{1C} by means of unique *Kpn*I and *Stu*I sites. A 44-residue amino-terminal truncation of the $Ca_V1.3$ α_{1D} subunit ($\alpha_{1D[NT\Delta]}$) was constructed similarly by PCR amplifying residues 45–180 from α_{1D} (ref. 32), followed by ligation into α_{1D} by means of unique *Nhe*I and *Bsi*WI sites. The mutant $\alpha_{1C[W82A]}$ was made by PCR amplifying α_{1C} residues 1–87, using a reverse primer containing a W82A mutation. This product was ligated into α_{1C} by means of unique *Hin*dIII and *Cla*I sites. The mutant $\alpha_{1D[W44A]}$ subunit was as described[19].

For FRET, all CFP–$NT_{B/C/D}$ constructs were made by PCR of desired segments of $\alpha_{1cBBBBb}$ or α_{1D}, followed by substitution of CaM_{WT} into a published CFP–CaM_{WT}/pcDNA3 clone[13], using unique *Not*I and *Xba*I sites. For fusion of CFP to the NSCaTE of the TonB-dependent receptor (TBDR; residues 464–484 of YP_242632.1), annealed synthetic primers encoding this motif (mammalian optimized) were ligated into unique *Not*I/*Xba*I sites of CFP–CaM_{WT}/pcDNA3. Throughout, all PCR-amplified segments were fully verified by sequencing.

Electrophysiology. HEK-293 cells were transiently transfected by using a calcium phosphate protocol[20]. Cells were cotransfected with 8 μg of rat brain β_{2a} (ref. 35), 8 μg of rat brain $\alpha_{2\delta}$ (ref. 36) and 1–8 μg of Ca^{2+} channel α_1 subunit. All α_{1C} and α_{1D} constructs were cotransfected with 2 μg of SV40 T antigen to enhance expression; 8 μg of cDNA for rat brain CaM_{12}, CaM_{34} or CaM_{1234} was added as required[20].

Room-temperature (20–22 °C) whole-cell recordings were performed 1–3 days after transfection, using Axopatch 200A/B amplifiers (Axon Instruments). P/8 leak subtraction was used, with series resistances of 1–2 MΩ after more than 70% compensation. Currents were filtered at 2 kHz (four-pole Bessel) and sampled at 10 kHz. For high-buffer experiments, internal solutions contained (in mM): caesium methanesulphonate, 114; $CsCl_2$, 5; $MgCl_2$, 1; MgATP, 4; HEPES (pH 7.4), 10; BAPTA, 10; at 295 mosM adjusted with caesium methanesulphonate. For low-buffer experiments, internal solutions contained (in mM): caesium methanesulphonate, 135; $CsCl_2$, 5; $MgCl_2$, 1; MgATP, 4; HEPES (pH 7.4), 10; EGTA, 0.5. In all experiments except those with $Ca_V1.2/1.3$, external solutions contained (in mM): tetraethylammonium methanesulphonate, 140; HEPES (pH 7.4), 10; $CaCl_2$ or $BaCl_2$, 5; at 300 mosM, adjusted with tetraethylammonium methanesulphonate. Because of lower $Ca_V1.2$ expression, 20 mM $CaCl_2$ or $BaCl_2$ was used. $Ca_V1.3$ recordings were made in 40 mM $CaCl_2$ or $BaCl_2$. A holding potential of −90 mV and a repetition interval of 60 s were used throughout. Data were analysed by custom MATLAB software (Mathworks); average data are shown as means ± s.e.m.

FRET two-hybrid assay. Fluorescence resonance energy transfer (FRET) two-hybrid experiments were performed in HEK-293 cells and analysed as described[13]. During imaging, the bath solution was a Tyrode's buffer containing 10 mM Ca^{2+}, to which 5 μM ionomycin (Sigma-Aldrich) was added for Ca^{2+}/CaM experiments. Concentration-dependent spurious FRET was subtracted from the raw data before binding-curve analysis[37].

Gel mobility-shift assay. We used a non-denaturing 13% acrylamide resolving gel, coupled with a 4% acrylamide stacking gel. $CaCl_2$ (100 μM) was added to the gel to maintain Ca^{2+}/CaM binding. Peptide samples were freshly solubilized into a sample buffer consisting of 20 mM Tris-HCl pH 6.8, 150 mM NaCl, 2% glycerol, 10 mM $CaCl_2$, 0.001% bromophenol blue dye and 2 μg of purified CaM protein[7]. Binding reactions (for 1 h) and electrophoresis were performed at about 0–4 °C in 25 mM Tris-HCl pH 8.4 and 200 mM glycine, with parameters of 50 V for 20 min, followed by 100 V for 2 h. Gels were stained over heat for 1 h with Coomassie R-250 (Bio-Rad) and destained overnight[20]. Peptides were synthesized by the Synthesis and Sequencing Facility at the Johns Hopkins School of Medicine. The wild-type NSCaTE peptide $NT_{C\text{-}peptide}$ was SWQAAIDAARQAKLMGS (rabbit α_{1C} sequence), and the mutant was SAQAAIDAARQAKLMGS. The IQ_A peptide was KIYAAMMIMEYYRQSKAKKLQ (based on the human α_{1A} subunit[2]). IQ_A peptide was added to Ca^{2+}/CaM in a molar ratio of 8:1 to produce a maximal binding shift. NSCaTE peptide was then added in various amounts (Fig. 2a).

Dansyl-CaM experiments. Purified recombinant CaM protein was dansylated with 0.5 mM dansyl chloride under alkaline conditions at room temperature (0.3 mM $CaCl_2$ for 4 h). The reaction was terminated with 5 mM hydroxylamine, and Tris buffer was added before dialysis against 10 mM MOPS (pH 7.2) at 4 °C (ref. 38). Peptides were as above. Spectrofluorimetry was conducted at 25 °C in 5 mM $CaCl_2$, 150 mM NaCl and 50 mM Tris-HCl pH 7.5. Peptide stocks were freshly prepared and used within 6 h. Dansyl-CaM (100 nM) was excited at 340 nm, and fluorescence was recorded from 400 to 650 nm (slit size 3 nm for excitation, 15 nm for emission; integration time 0.1 s), with a Fluorolog-3 spectrofluorimeter (Horiba Jobin Yvon). No detectable bleaching was observed in controls. Binding curves were determined from the average of five 490-nm measurements (F_{490}) at each peptide concentration. Subtraction of background fluorescence used a correction factor ($m_{peptide}$) derived from measurements of peptide alone ($F_{490,bg\text{-}corrected} = F_{490} - m_{peptide} \cdot [peptide]$). We calculated $F_{490,full\text{-}corrected}$ as $F_{490,bg\text{-}corrected} \times V_{tot}/V_{initial}$ (where V_{tot} is the final volume and $V_{initial}$ was 2.5 ml), to correct for dilution by successive peptide additions. Fractional binding (B) was $(F_{490,full\text{-}corrected,max} - F_{490,full\text{-}corrected})/(F_{490,full\text{-}corrected,max} - F_{490,full\text{-}corrected,min})$; least-square fits were performed with $B = [peptide]^k/([peptide]^k + K_d{}^k)$, with resulting $k \approx 1$.

31. Agler, H. L. *et al.* G protein-gated inhibitory module of N-type ($Ca_V2.2$) Ca^{2+} channels. *Neuron* **46**, 891–904 (2005).
32. Xu, W. & Lipscombe, D. Neuronal $Ca_V1.3\alpha_1$ L-type channels activate at relatively hyperpolarized membrane potentials and are incompletely inhibited by dihydropyridines. *J. Neurosci.* **21**, 5944–5951 (2001).
33. Williams, M. E. *et al.* Structure and functional expression of an omega-conotoxin-sensitive human N-type calcium channel. *Science* **257**, 389–395 (1992).
34. Wei, X. Y. *et al.* Heterologous regulation of the cardiac Ca^{2+} channel α1 subunit by skeletal muscle β and γ subunits. Implications for the structure of cardiac L-type Ca^{2+} channels. *J. Biol. Chem.* **266**, 21943–21947 (1991).
35. Perez-Reyes, E. *et al.* Cloning and expression of a cardiac/brain β subunit of the L-type calcium channel. *J. Biol. Chem.* **267**, 1792–1797 (1992).
36. Tomlinson, W. J. *et al.* Functional properties of a neuronal class C L-type calcium channel. *Neuropharmacology* **32**, 1117–1126 (1993).
37. Stratton, J., Evans, J., Erickson, M. G., Alvania, R. S. & Yue, D. T. The nature of concentration-dependent spurious FRET arising from CFP and YFP. *Biophys. J.* **86**, 317a (2004).
38. Kincaid, R. L., Billingsley, M. L. & Vaughan, M. Preparation of fluorescent, cross-linking, and biotinylated calmodulin derivatives and their use in studies of calmodulin-activated phosphodiesterase and protein phosphatase. *Methods Enzymol.* **159**, 605–626 (1988).